# Controlled LCST Behavior and Structure Formation of Alternating Amphiphilic Copolymers in Water

E. Kostyurina[1], J.U. De Mel[2], A. Vasilyeva[1], M. Kruteva[1], H. Frielinghaus[3], M. Dulle[1], L. Barnsley[3,4], S. Foerster[1,3], G.J. Schneider[2,5], R. Biehl[1*], J. Allgaier[1*]

[1]*Forschungszentrum Jülich GmbH, Jülich Centre for Neutron Science (JCNS-1) and Institute for Biological Information processing (IBI-8), Jülich, Germany*

[2]*Louisiana State University, Department of Chemistry, Baton Rouge, Louisiana, United States*

[3]*Forschungszentrum Jülich GmbH, Jülich Centre for Neutron Science at MLZ, Garching, Germany*

[4]*Australian Synchrotron, ANSTO, Clayton, Victoria, Australia*

[5]*Louisiana State University, Department of Physics & Astronomy, Baton Rouge, Louisiana, United States*

## ABSTRACT

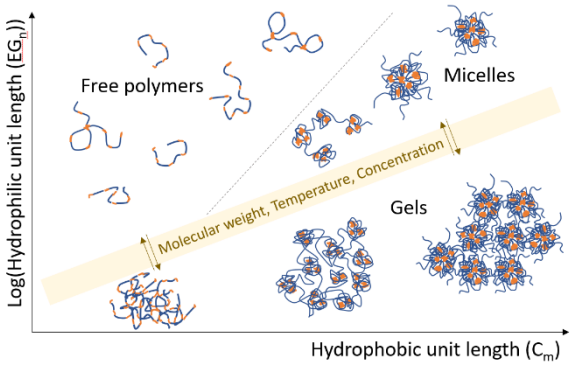


Amphiphilic polymers show a rich self-assembly behavior in aqueous solutions. In experimental investigations statistical copolymer or block copolymer architectures are usually investigated, because of their ease of synthesis or their structural analogy to surfactants. A copolymer structure that links the two architectures are alternating copolymers, which are easily accessible by polycondensation reactions. Using alternating hydrophilic and hydrophobic building blocks with varying length allows a systematic variation between statistical and multi-block architectures. We synthesized alternating amphiphilic copolymers as polyesters using hydrophobic dicarboxylic acids ($C_4$ – $C_{20}$) and hydrophilic polyethylene glycol (PEG) units ($EG_3$ – $EG_{1000}$). Copolymers with long EG units were made accessible with the help of a newly developed esterification process. The solution properties of the amphiphilic copolymers feature a lower critical solution temperature (LCST) behavior in water, which can be systematically varied over a wide range from 3 – 83°C by adjusting the lengths of the $C_n$- and $EG_m$–units. We find that the transition temperature depends linearly on the hydrophobic unit length $C_m$ and logarithmically on the hydrophilic length $EG_n$. In the one-phase region the PEG copolymer coils are more compact compared to the respective PEG homopolymers due to hydrophobic interactions between the hydrophobic units leading to loop formation. For shorter PEG-units the copolymers form micellar structures consisting only of a few copolymer chains. The micellar cores consist of hydrophobic regions containing only a few dicarboxylic acid units, embedded in a PEG-rich and water-poor matrix. The cores are surrounded by a rather diluted corona of PEG chains. Further decreasing the PEG unit length leads to the formation of highly swollen gels consisting of networks of interconnected micelles. These can self-assemble to form highly ordered liquid crystalline cubic phases. The study demonstrates how the structure of alternating amphiphilic copolymers can be systematically varied to adjust thermal solution properties such as the LCST

over a wide range, as well as the self-assembly properties varying between single chain, micelle, gels and highly ordered lyotropic liquid crystals.

## 1. Introduction

Amphiphilic polymers have been largely investigated in aqueous media with respect to micellization or interfacial properties. They play an important role in many applications. So far, from the structural standpoint, the focus was on diblock- and triblock- along with comb-shaped polymers and hydrophilic polymers, end-capped with low molecular weight hydrophobic units.[1,2] Alternating amphiphilic polymers (AAPs) have been in the focus of interest to a much smaller degree, because their synthesis is restricted to special monomers or yields polymers having a broad molecular weight distribution (MWD). In aqueous media, these polymers frequently form complex structures.

The hydrophobic and hydrophilic units in AAPs can be low molecular weight monomers or large polymeric blocks. In the latter case multiblock copolymers are formed. AAPs with monomeric hydrophobic and hydrophilic units are accessible for example via alternating polymerization of maleic anhydride with styrene or vinyl ether monomers.[3–5] The anhydride hydrolysis under basic conditions yields ionic moieties and the hydrophobic functionality frequently is located in the co-monomer side chains. Alternatively, polycondensation reactions of dicarboxylic acids with dialcohols or diamines of opposite polarity have been applied to synthesize AAPs.[6–10] Other procedures like click chemistry have been reported in rare cases.[11] The access to AAPs with polymeric hydrophilic and hydrophobic units is limited to a small number of methods. Condensation reactions, as outlined above, were used to synthesize AAPs, containing for example alternating ethylene oxide (EO) and propylene oxide (PO) units.[12–14] In a different approach, controlled radical polymerization techniques were applied to produce AAPs of hydrophobic and hydrophilic methacrylate monomers.[15,16]

AAPs were examined in aqueous media with respect to their solution behavior and structure formation. If the hydrophilic units dominate, water-soluble polymers are obtained, which frequently show a lower critical solution temperature (LCST) behavior.[6,15,16] Furthermore, the formation of micelles was reported. Mostly various flower-like structures were found.[3,4,9,10,12–16] A few works reported nanotube or vesicle formation.[7,11] In agreement with the experimental results, different simulation studies predicted the existence of globular or expanded free chains and a large variety of complex micellar structures like uni- and multi-flower-like or worm-like micelles and micellar chains.[17–21] In addition, the formation of gels was reported.[19] The structures formed strongly depend on solvent quality and the sizes and the size ratio of the hydrophobic units.

Thermo-responsive polymers are highly desirable in a wide range of applications.[22,23] For example, they have a significant presence in drug delivery applications.[23–25] Many polymers are used with other molecules to obtain co-functionalities and build multifunctional materials.[26] One of the most versatile and popular polymers in this regard is poly(N-isopropylacrylamide) (PNIPAM) and PNIPAM derivatives.[27–29] Poly(2-oxazoline)s[30] as well as random copolymers of EO with comonomers like propylene oxide[31] and other epoxide monomers[32] allow to vary the LCST behavior over a broad temperature range by modifying

the monomer side groups or polymer composition. The same holds for AAPs, where the selection of the hydrophobic and hydrophilic units allows to predict the LCST behavior.[33] In this work we synthesized polyesters from commercially available dicarboxylic acids and PEG units. These AAPs show a LCST behavior, which can be predetermined by the selection of the hydrophilic and hydrophobic moieties. Using small angle neutron scattering (SANS) and small angle X-ray scattering (SAXS) techniques, the structures formed in water were studied over a broad range of unit sizes and compositions.

## 2. Experimental Methods

**Polymer synthesis.** The AAPs were synthesized as polyesters using dicarboxylic acids and polyethylene glycols. The products were obtained by direct esterification of the diacids and diols under the removal of water or by activating the diacid first with the help of 1,1'-carbonyldiimidazole (CDI). Some of the polymers were fractionated to obtain samples with narrow molecular weight distributions. All synthetic procedures are described in detail in the Supplementary Information (SI).

**Polymer Characterization.** Size-exclusion chromatography (SEC) experiments were carried out using an Agilent 1260 Infinity SEC instrument equipped with a Wyatt DAWN Heleos II light scattering (LS) detector, an Optilab T-rex differential refractive index (RI) detector and with three PolyPore columns at 50 °C. The solvent was a mixture of THF, DMA, and acetic acid (84:15:1 by volume) at a flow rate of 1 mL/min. NMR spectra were collected on a Bruker Avance III 600 MHz spectrometer equipped with a Prodigy cryoprobe with a 5 mm PFGAutoX DB probe. Samples were measured at 295 K. The molecular weights of the PEG units were determined from $^{1}$H-NMR spectra in pyridine-$d_5$. $M_n$ values were calculated from the signal intensities of the methylene units next to the alcoholic end groups at 3.95 ppm and the rest of the PEG signals between 3.5 and 3.7 ppm.[34]

**Cloud point temperature (CPT) determination.** Non-fractionated polymers were dissolved in deionized water at a concentration of 10 mg/mL. Samples of about 5 mL were gradually heated in a thermostated shaker and visually inspected. The temperature, where turbidity appeared was taken as the CPT. For the fractionated samples the CPT was measured by dynamic light scattering (DLS). The polymers were dissolved in deionized water in a concentration of 10 mg/mL and analyzed in a wide temperature range with a step of 1°C. CPT was detected as the appearance of large aggregates. All the DLS measurements were performed with a Malvern Zetasizer Nano ZS apparatus with a backscattering set up ($\theta$ = 173°) and a He-Ne laser of the wavelength $\lambda$ = 633 nm.

**Hydrodynamic radius ($R_H$) determination.** The $R_H$ of the AAPs was determined using the Malvern Zetasizer Nano ZS instrument described above. The $R_H$ value was obtained by analyzing autocorrelation functions using a built-in algorithm of the instrument.

**Small Angle Neutron Scattering (SANS).** SANS experiments were performed at the instrument KWS-1[35,36] operated by the Jülich Centre for Neutron Science (JCNS) at Heinz Meier-Leibnitz Zentrum (MLZ) in Garching, Germany. The incident neutron wavelength $\lambda$ was 0.5 nm ($\Delta\lambda/\lambda$ = 10%). The data were obtained from two different detector and collimation distances: the

detector distances of 1.5 m with a collimation distance of 4 m and 8 m with a collimation distance of 8 m. The resulting Q-range was 0.06 – 4 $nm^{-1}$. Here Q is the magnitude of the scattering wave vector defined as $Q = (\frac{4\pi}{\lambda})\sin(\theta)$, where $2\theta$ is the angle between the incident and scattered beam. The polymers were dissolved in $D_2O$ at a concentration of 5 or 10 mg/mL and measured in quartz cells with a beam path of 1 mm. The temperature was controlled by a thermostat. The data presented here were converted to an absolute intensity unit of $cm^{-1}$ taking into account the sample thickness, transmission, the scattering from a standard sample and the background from electronic noise, the solvent and the quartz cell. Data reduction was done using the QtiKWS software[37] and data analysis has been done using the Python-based project Jscatter.[38]

**Small angle X-ray Scattering (SAXS).** SAXS experiments were performed the Jülich Centre for Neutron Science (JCNS) at Forschungszentrum Jülich, Germany. The instruments "Ganesha-Air" from SAXSLAB/XENOCS and Gallium Anode Low-Angle X-ray Instrument (GALAXI)[39] were used. The X-ray source of the laboratory-based "Ganesha-Air" system is a D2-MetalJet (Excillum) with a liquid metal anode operating at 70 kV and 3.57 mA with Ga− Kα radiation (wavelength λ = 0.13414 nm). The beam is further focused with a focal length of 55 cm, using specially made X-ray optics (Xenocs) to provide a very narrow and intense beam at the sample position. Two pairs of scatterless slits are used to adjust the beam size depending on the detector distance. The data were acquired with a position-sensitive detector (PILATUS 300 K, Dectris). After calibration with silver behenate, the distance from the sample to the detector was set to 950 and 350 mm resulting in a Q-range 0.13 – 6 $nm^{-1}$. The GALAXI X-ray source is a liquid anode of a GaInSn alloy operating at 70 keV with Ga− Kα radiation (wavelength λ = 0.134 nm). Two four-segment slits which are separated by 4 m distance collimate the beam and confine the size to about 0.7 × 0.7 $mm^2$. A third slit reduces the scattering from the edges of the second one. A sample-to-detector distance of 1285 mm calibrated using Bragg reflections from silver behenate resulting in a Q-range of 0.09–4 $nm^{-1}$ was used. All samples were sealed in glass capillaries of 2 mm inner diameter. Data analysis was done using the Python-based project Jscatter.[38]

## 3. Results and discussion

### 3a. Synthesis

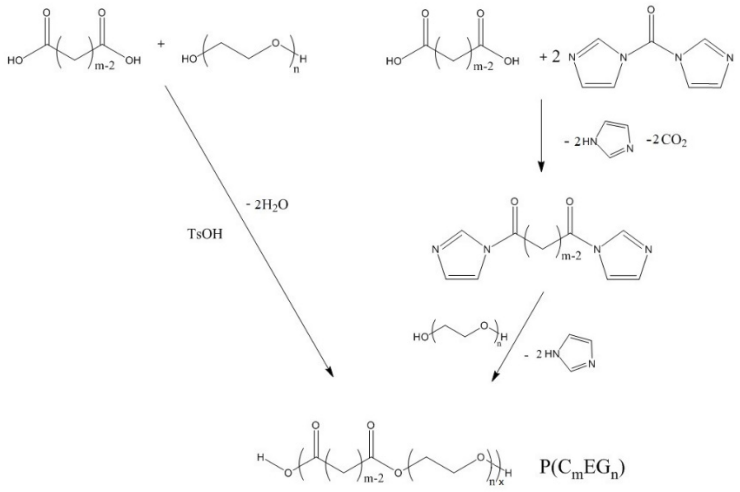


*Figure 1. Synthesis of AAPs via polycondensation using hydrophobic dicarboxylic acids and hydrophilic polyethylene glycols as monomers. The polymer chain ends are equipped with carboxylic acid and alcohol groups in a random fashion.*

The AAPs $P(C_mEG_n)$ used in this work contain alternating hydrophobic and hydrophilic units. Dicarboxylic acids ($C_m$) were used as hydrophobic units and polyethylene glycols ($EG_n$) as the hydrophilic ones (see Figure 1). The total number of carbon atoms in the diacids is given by m and the number of EG repeat units in the PEGs is specified by n. PEGs contain two alcohol end groups and except tri- and tetraethylene glycol have a molecular weight distribution (MWD). The molecular weight (MW) characterization of the compounds used is summarized in Table 1.

**Table 1. Hydrophobic and hydrophilic units used for the synthesis of the AAPs.**

| dicarboxylic acid (m) | | MW | PEG (n) | | $M_n$, g/mol | $M_w/M_n$ |
|---|---|---|---|---|---|---|
| succinic acid | ($C_4$) | 118 | triethylene glycol | ($EG_3$) | 150 | |
| glutaric acid | ($C_5$) | 132 | tetraethylene glycol | ($EG_4$) | 194 | |
| adipic acid | ($C_6$) | 146 | PEG 300 | ($EG_6$) | 284 | n.d. |
| suberic acid | ($C_8$) | 174 | PEG 400 | ($EG_9$) | 400 | n.d. |
| sebacic acid | ($C_{10}$) | 202 | PEG 600 | ($EG_{13}$) | 599 | 1.05 |
| dodecanedioic acid | ($C_{12}$) | 230 | PEG 1k | ($EG_{22}$) | 986 | 1.04 |
| tetradecanedioic acid | ($C_{14}$) | 258 | PEG 2k | ($EG_{47}$) | 2,110 | 1.04 |
| eicosanedioic acid | ($C_{20}$) | 343 | PEG 4.5k | ($EG_{103}$) | 4,530 | 1.03 |
| | | | PEG 10k | ($EG_{240}$) | 10,600 | 1.01 |
| | | | PEG 45k | ($EG_{1000}$) | 44,200 | 1.04 |

Most of the AAP syntheses using succinic anhydride ($C_4$) and $C_5$ to $C_{12}$ dicarboxylic acids with lower MW PEGs up to $EG_{22}$ were achieved by polycondensation while removing the reaction water via azeotrope distillation or vacuum. *p*-Toluenesulfonic acid (TsOH) was used as catalyst (Figure 1, left side). The synthetic details are given in the SI and the MW characterization as

well as the average number of hydrophobic-hydrophilic repeat units per polymer chain (x) is summarized in Table 2.

**Table 2. SEC/LS characterization results for the non-fractionated AAPs; x represents the number of hydrophobic/hydrophilic repeat units.**

| | $M_n$, g/mol | $M_w/M_n$ | x |
|---|---|---|---|
| $P(C_4EG_3)$ | 8,790 | 1.82 | 53.8 |
| $P(C_4EG_4)$ | 19,360 | 1.95 | 66.3 |
| $P(C_4EG_6)$ | 6,590 | 1.58 | 17.9 |
| $P(C_5EG_3)$ | 3,760 | 1.28 | 15.2 |
| $P(C_5EG_4)$ | 7,220 | 1.75 | 24.8 |
| $P(C_5EG_6)$ | 11,700 | 1.51 | 30.7 |
| $P(C_5EG_{13})$ | 6,390 | 1.52 | 9.2 |
| $P(C_6EG_6)$ | 8,700 | 1.59 | 22.0 |
| $P(C_8EG_6)$ | 5,610 | 1.65 | 13.2 |
| $P(C_8EG_9)$ | 5,130 | 1.87 | 9.5 |
| $P(C_8EG_{13})$ | 6,790 | 1.58 | 9.1 |
| $P(C_8EG_{22})$ | 11,400 | 2.08 | 10.1 |
| $P(C_{10}EG_{13})$ | 6,040 | 1.46 | 7.9 |
| $P(C_{10}EG_{22})$ | 10,100 | 1.49 | 8.7 |
| $P(C_{12}EG_{13})$ | 5,270 | 1.66 | 6.6 |
| $P(C_{12}EG_{22})$ | 20,100 | 1.63 | 17.0 |
| $P(C_{14}EG_{47})$ | 91,100 | 1.45 | 38.7 |
| $P(C_{14}EG_{103})$ | 168,000 | 1.47 | 35.1 |
| $P(C_{20}EG_{47})$ | 60,000 | 1.68 | 24.6 |
| $P(C_{20}EG_{103})$ | 114,000 | 1.47 | 23.5 |
| $P(C_{20}EG_{240})$ | 231,000 | 1.21 | 21.2 |
| $P(C_{20}EG_{1000})$ | 537,000 | 1.68 | 12.1 |

For larger PEG units ($EG_{47}$ and higher) the polyester synthesis via water removal failed. No more than oligomeric products were obtained because of the increasingly lower concentrations of reactive groups. The replacement of the dicarboxylic acid by the acid chloride analog did not improve the situation. Only the activation of the carboxylic acid with the help of CDI proofed successfully. The activation of carboxylic acids with CDI for esterification or amidation reactions is a standard procedure in organic synthesis.[40] In this approach a dicarbonylimidazole is formed intermediately (see Figure 1, right side), which reacts with PEG under formation of the AAP. As a result, polymerization degrees between 20 to 40 hydrophobic-hydrophilic repeat units could be achieved (Table 2). The same procedure was applied for the synthesis of a $P(C_{10}EG_{22})$ polymer in order to obtain samples of higher polymerization degrees. The CDI activation procedure demands dry reaction conditions because of the water sensitivity of CDI. In addition, the exact stoichiometry is required of all three components dicarboxylic acid, PEG, and CDI. With increasing PEG MW, this gets a challenging task due to the limited precision of the MW determination. NMR end-group analysis in pyridine-$d_5$ proved to be the most precise method for this purpose.[34]

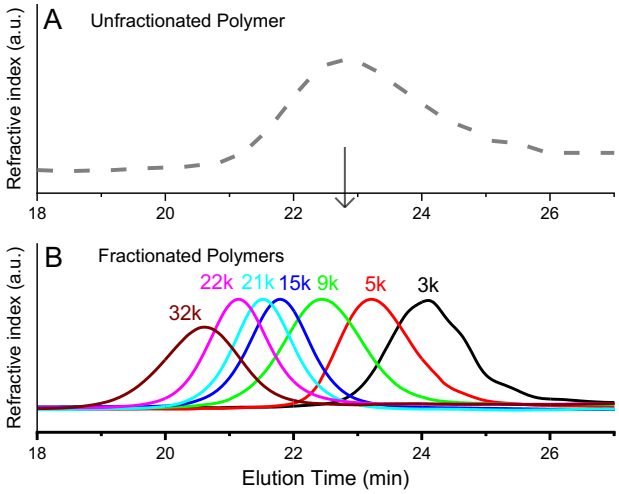


*Figure 2. A: SEC trace of P($C_8EG_{13}$) after the polymerization reaction. B: SEC traces of P($C_8EG_{13}$) samples after fractionation; molecular weights corresponding to the sample names from Table 3 are shown above each curve.*

Most of the polymerizations based on CDI were executed in a one-pot synthesis by first activating the dicarboxylic acid and then adding the PEG. Only the synthesis of P($C_{20}EG_{1000}$) was carried out in a modified way. Because of the high MW of the PEG unit of about 45k, the concentration of reactive groups is on the same level as the water concentration of a dry solvent. Therefore, the dicarboxylic acid was first activated with an excess of CDI and the dicarbonylimidazole intermediate product was isolated and purified prior to the polymerization with PEG. In addition, 1,8-diazabicyclo[5.4.0]undec-7-en (DBU) was added as catalyst[41,42] in the polymerization step.

The polymerization products by nature exhibit a broad MWD. Some of the raw products were fractionated in order to obtain polymers with different MW and narrower MWD. The fractionations were carried out either in a single solvent by exploiting the temperature dependent solubility of the polymer or by using a solvent/non-solvent pair. As a result, fractions of several grams were obtained, most of them having a MWD between 1.1 and 1.2. The details are described in the SI. Exemplarily, the SEC traces of the P($C_8EG_{13}$) polymerization product before fractionation and the fractionated samples are shown in Figure 2. The MW characterization of the samples fractionated in this way is listed in Table 3.

All AAPs containing PEG units of 2k and higher exhibit high MWs. In this case, molecular weight fractionation is difficult due to the small MW dependence of the solubility. For this reason, these polymers were only fractionated in a simple approach by adding stepwise non-solvent to a diluted polymer solution and fractions with MWDs between 1.2 and 1.7 were obtained. The synthetic details are described in the SI. The MW characterization is listed in Table 4.

**Table 3. SEC/LS characterization results of the fractionated AAPs; x represents the number of hydrophobic/hydrophilic repeat units.**

| | $M_n$, g/mol | $M_w/M_n$ | x |
|---|---|---|---|
| $P(C_4EG_4)33k$ | 33,100 | 1.29 | 119.7 |
| $P(C_4EG_4)21k$ | 20,800 | 1.13 | 75.2 |
| $P(C_4EG_4)11k$ | 10,500 | 1.10 | 37.9 |
| $P(C_4EG_4)4k$ | 4,140 | 1.08 | 14.9 |
| $P(C_4EG_4)2k$ | 2,070 | 1.05 | 7.4 |
| $P(C_5EG_6)80k$ | 80,200 | 1.15 | 202.5 |
| $P(C_5EG_6)40k$ | 39,500 | 1.10 | 99.7 |
| $P(C_5EG_6)26k$ | 25,500 | 1.15 | 64.4 |
| $P(C_5EG_6)18k$ | 18,400 | 1.10 | 46.5 |
| $P(C_5EG_6)12k$ | 11,800 | 1.10 | 29.8 |
| $P(C_5EG_6)7k$ | 6,600 | 1.11 | 16.7 |
| $P(C_5EG_6)4k$ | 4,400 | 1.10 | 11.1 |
| $P(C_5EG_6)2k$ | 2,400 | 1.07 | 6.1 |
| $P(C_8EG_{13})33k$ | 32.600 | 1.22 | 44.2 |
| $P(C_8EG_{13})22k$ | 22,100 | 1.18 | 29.9 |
| $P(C_8EG_{13})21k$ | 20,700 | 1.17 | 28.0 |
| $P(C_8EG_{13})15k$ | 15,100 | 1.15 | 20.5 |
| $P(C_8EG_{13})9k$ | 8,790 | 1.16 | 11.9 |
| $P(C_8EG_{13})5k$ | 4,720 | 1.17 | 6.4 |
| $P(C_{10}EG_{22})65k$ | 65,100 | 1.19 | 55.7 |
| $P(C_{10}EG_{22})47k$ | 47,300 | 1.11 | 40.5 |
| $P(C_{10}EG_{22})35k$ | 34,900 | 1.07 | 29.9 |
| $P(C_{10}EG_{22})25k$ | 25,400 | 1.07 | 21.7 |
| $P(C_{10}EG_{22})13k$ | 13,300 | 1.15 | 11.4 |

**Table 4. SEC/LS characterization results for the AAPs containing PEG units of 2k and longer; x represents the number of hydrophobic/hydrophilic repeat units.**

| | $M_n$ ,g/mol | $M_w/M_n$ | x |
|---|---|---|---|
| $P(C_{14}EG_{47})98k$ | 98,100 | 1.37 | 41.7 |
| $P(C_{14}EG_{47})41k$ | 41,400 | 1.17 | 17.6 |
| $P(C_{14}EG_{47})16k$ | 15,600 | 1.26 | 6.6 |
| $P(C_{14}EG_{103})174k$ | 174,000 | 1.40 | 36.3 |
| $P(C_{14}EG_{103})48k$ | 47,900 | 1.59 | 10.0 |
| $P(C_{20}EG_{47})113k$ | 113,000 | 1.32 | 46.4 |
| $P(C_{20}EG_{47})79k$ | 78,500 | 1.31 | 32.2 |
| $P(C_{20}EG_{47})32k$ | 31,900 | 1.48 | 13.1 |
| $P(C_{20}EG_{103})161k$ | 161,000 | 1.20 | 33.2 |
| $P(C_{20}EG_{103})81k$ | 81,400 | 1.30 | 16.8 |
| $P(C_{20}EG_{103})49k$ | 49,300 | 1.20 | 10.2 |
| $P(C_{20}EG_{240})228k$ | 228,000 | 1.32 | 20.9 |
| $P(C_{20}EG_{1000})663k$ | 663,000 | 1.75 | 14.9 |
| $P(C_{20}EG_{1000})168k$ | 168,000 | 1.51 | 3.8 |

## 3b. Hydrolytic stability of the AAPs

Ester bonds are susceptible to hydrolysis. In the case of polymers this can cause chain scission reactions and decomposition of the polymer structure. For this reason, the hydrolytic stability of narrowly distributed P($C_8EG_{13}$)22k (see Table 3) was tested by taking samples of aqueous solutions after different times. The samples were freeze-dried and examined by SEC. The results are shown in Figure 3. At room temperature the hydrolytic degradation is very slow. Even after 6 weeks the signal shape remained almost unchanged. The small shift to higher elution times might indicate a minimal degree of hydrolysis. On the contrary, the degradation process is visibly faster at 40 °C. At this temperature, the SEC examination revealed a small low MW tailing already after 2 weeks and a visibly reduced MW after 6 weeks. At 60 °C first signs of hydrolysis appear within the first week. After 6 weeks the refractive index signal vanished almost completely. These hydrolysis results show that the polymers are sufficiently stable in aqueous solution in the temperature and time range of our measurements. Only at high temperatures degradation has to be considered.

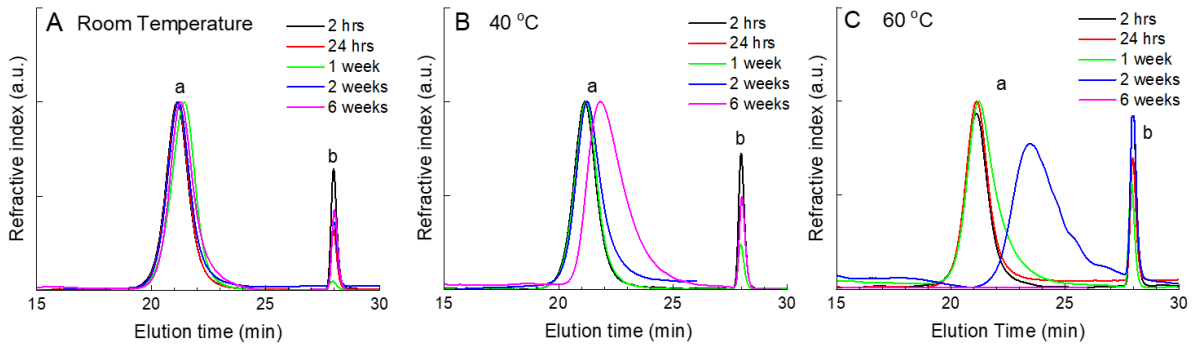


*Figure 3. Hydrolytic stability tests in aqueous solution measured by SEC. P($C_8EG_{13}$)22k of the concentration 10 mg/mL in water was used for the experiments. Signal "a" represents the polymer signal, sighnal "b" represents a flow rate marker. The experiments were performed at three different temperatures: A: Room temperature, B: 40 °C, C: 60 °C.*

## 3c. Solubility and thermal behavior of the polymers in water

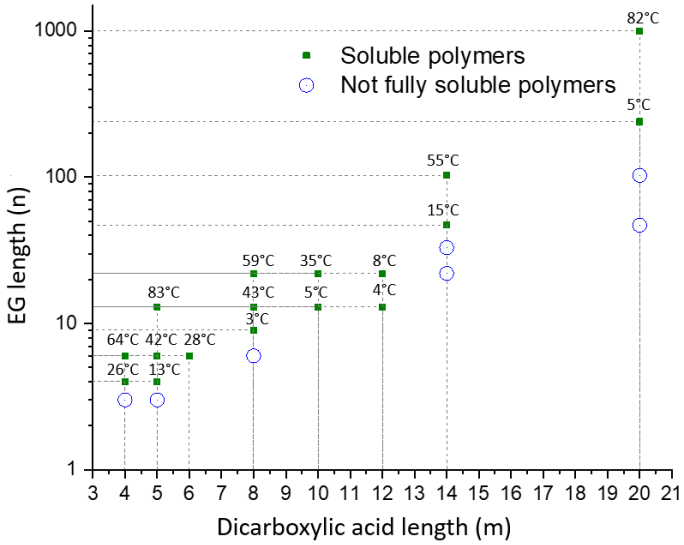


*Figure 4. Illustration of solubilities and cloud points for different lengths of the hydrophobic and the hydrophilic units at a concentration of 10 mg/mL in water. For fully water-soluble polymers the CPT is indicated above the corresponding point.*

The water solubility of the AAPs was first measured by screening experiments over a broad range of polymer compositions using the non-fractionated polymers listed in Table 2. The results for a polymer concentration of 10 mg/mL are collected in Figure 4, where the chain length of the dicarboxylic acid is plotted against the PEG ethoxylation degree. The CPTs are given for fully soluble polymers. With increasing ethoxylation degree and overall hydrophilicity of the polymers, the CPT moves to higher temperatures. Larger dicarboxylic acid units require increasingly longer PEG units in order to keep the polymers water-soluble. For $C_{14}$ and $EG_{47}$ unit ($M_n$ = 2,110 g/mol) is needed and in the case of $C_{20}$, $EG_{240}$ ($M_n$ = 10,600 g/mol) units are required to obtain at least solubility at low temperatures. Interestingly, the LCST behavior still exists for the highest PEG unit investigated in this work of $EG_{1000}$ ($M_n$ = 44,200 g/mol). Although the fraction of the hydrophobic unit in P($C_{20}EG_{1000}$) is below 1 mass-%, the CPT of this material is 82°C. Pure PEG for comparison exhibits a LCST value above 100 °C.[43]

The CPT depends strongly on the molecular weight and the concentration. This is shown exemplarily for P($C_4EG_4$) with fractionated samples of different molecular weights (Table 3) in Figure 5A. At lower numbers of hydrophilic-hydrophobic repeat units there is a strong temperature dependence, which gets almost constant at higher chain lengths. The same holds for the concentration dependence which was measured between 5 and 100 mg/mL. Similar behavior was observed previously for alternating amphiphilic polymers.[6,12,33] For other polymer compositions we tested the thermal behavior is qualitatively similar (see Figure 5B).

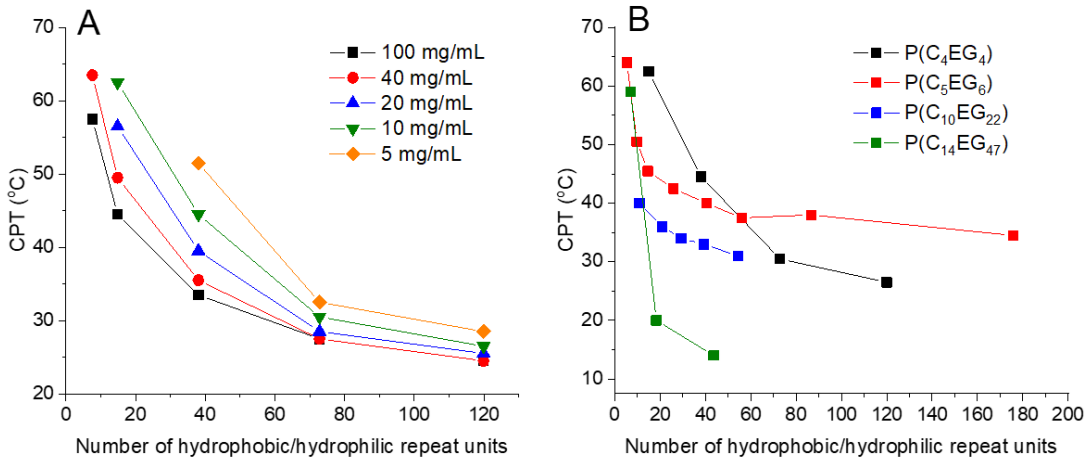


*Figure 5. A: Dependence of the CPT on the number of hydrophobic/hydrophilic repeat units and concentration for P($C_4EG_4$) polymer; B: Dependence of the CPT on the number of hydrophobic/hydrophilic repeat units for different polymer compositions at a concentration of 10 mg/mL.*

The thermal examination of the non-fractionated samples (Figure 4) was done with polymers of very different molecular weights (Table 2). As the thermal properties strongly depend on the molecular weight, the question arises, whether the CPTs for the different polymers are comparable. As these polymers were not fractionated they exhibit a broad MWD. As the CPTs were determined as the temperature of the turbidity onset, they correspond to the highest MW fractions, which get insoluble first (see Figure S2). Accordingly, for all the fractionated polymers the CPT of the highest chain lengths are in good agreement with the values measured for the broadly distributed samples and therefore are close to the LCST values.

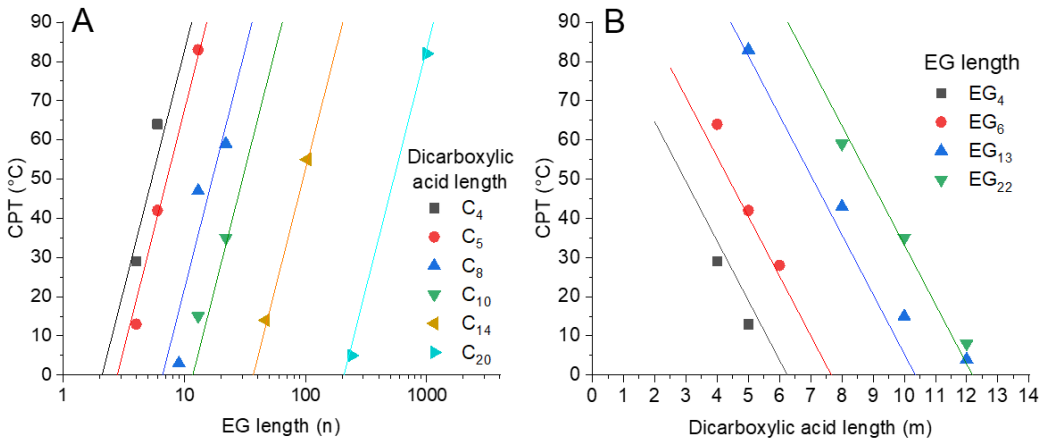


*Figure 6. A: Dependence of the CPT on the EG unit length at fixed dicarboxylic acid length. Lines represent the fit results assuming the same slope for all the curves; B: Dependence of the CPT on the dicarboxylic acid length at fixed EG length. Lines are calculated from equation 1.*

More details are illustrated in Figure 6, by plotting CPT as a function of the number of the EG length, and the dicarboxylic acid length. The dependence of the CPT on the EG length is logarithmic, whereas the dependence on the dicarboxylic acid length is weaker and shows a linear behavior (Figure 6). As a consequence, the ratio of the EG and C numbers must be

considerably increased with increasing the C number, to obtain water-soluble polymers or to stay at the same LCST. From the data shown in Figure 6 the CPT can be calculated as a function of $C_m$ and $EG_n$. Assuming the same slope for all the dicarboxylic acid lengths (m) in Figure 6A, and a linear dependence of the intercept on m, we get the following equation for the CPT determination:

$$CPT = 53.0[\pm 4.1] \cdot \ln(n) - 15.2[\pm 1.2] \cdot m + 21.6[\pm 4.3] \quad (1)$$

The lines in Figure 6B are calculated from this equation with fixed PEG lengths n. This empirical finding might be related to the Gibbs free energy of mixing.[44] In the Gibbs free energy the entropy of the polymer chain is described by a logarithmic contribution dependent on the chain length. In our case the entropic term is dominated by the EG unit length. The enthalpy contribution is proportional to the interaction between polymer and solvent. The interaction energy between the hydrophobic units and water is much larger compared to the other interactions in this system leading to the linear dependence on *m*.

It is interesting to notice that a very similar dependence of the CPT on the hydrophobic unit length was observed for the other methylene-PEG based amphiphilic polymers,[33] where the slope values were 15.01[±0.24] and 15.66[±0.31] for different polymer compositions. In summary, the AAP solubility in water strongly depends on the lengths of the hydrophilic and hydrophobic units, the composition as well as the MW and the concentration. With the knowledge of the compositional influence on the thermal behavior, the LCST properties of a polymer can be tuned basically between the freezing and the boiling point of water. The only limiting factor is the reduced long-term hydrolytic stability at high temperatures.

When the PEG units are not long enough to keep the polymers water-soluble, the polymers form micellar structures or macroscopic gels. A detailed structural description is given in the next chapter. The water adsorption of non-soluble polymers equipped with short hydrophilic units is small, e.g. 70% of the polymer weight for P($C_8EG_6$). However, the water uptake for polymers containing $C_{14}$ and especially $C_{20}$ hydrophobic units increases drastically due to the much longer PEG units. The maximum swelling degrees, for the polymers equipped with $C_{14}$ and $C_{20}$ hydrophobic units are shown in Figure 7A. For these experiments the polymer fractions with the highest MWs were used. The swelling degree is calculated as the ratio of the gel weight to the weight of the dry polymer. For polymers containing shorter PEG units the water uptake is not so pronounced, however, the gels formed are mechanically fairly stable. More information is given in the SI (Figure. S3). With longer PEG units the swelling degree increases strongly. It reaches a value of 37 for P($C_{20}EG_{240}$)228k. Due to the high water content the mechanical stability of this gel is poor which makes it soft and mechanically unstable. The same behavior is observed for the $C_{14}$ polymers, which generally show a higher swelling degree than the $C_{20}$ materials.

The gels always coexist with a soluble fraction. The amount of soluble polymer depends on the composition and the molecular weight (Figure 7B). The more the PEG units dominate and the lower the overall MW is, the higher is the soluble fraction. Generally, the molecular weight of the soluble polymer fraction is visibly lower than the one of the starting material. This is demonstrated with the SEC analysis for P($C_{20}EG_{103}$)81k in the SI (Figure S3).

More detailed information about the soluble fractions and the swelling degrees of all the examined polymers can be found in the SI (Table. S7).

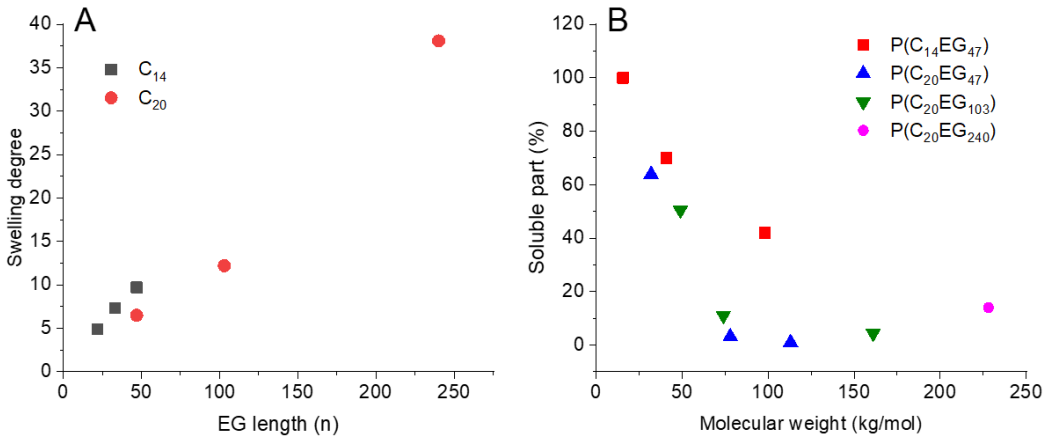


*Figure 7. Gel forming AAPs. A: Dependence of the swelling degree on the EG length. The fractions with the highest molecular weights were used for each composition; B: Dependence of the soluble fraction on the composition and molecular weight.*

## 3d. Structural properties of the polymers in water

### Soluble polymers

The alternating structure of the polymers and their LCST behavior stimulate interest in the question which structures such polymers can form in water. We performed a detailed study of the structural properties covering various polymer compositions, molecular weights and temperatures.

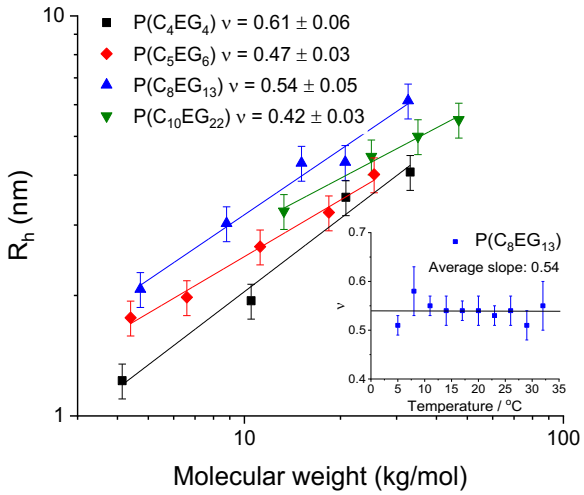


*Figure 8. Dependence of the hydrodynamic radius ($R_h$) on the molecular weight for different polymer compositions at 25C. Solid lines represent the fits using $R_h \sim MW^{\nu}$. Insert: Dependence of the Flory parameter ν on temperature for the polymer composition $P(C_8EG_{13})$.*

As a first step, the structure formation of AAPs in water was examined by dynamic light scattering (DLS). The concentration was always 5 mg/mL, which is below the overlap concentration for all the investigated polymers, and only the temperatures below the CPT

were taken into account. For most of the examined AAP solutions a very small fraction of large-scale aggregates (>100 nm) was detected, which was also observed for pure PEG.[45] The main fraction was attributed to single polymer chains with a reasonable hydrodynamic radius as shown in Figure 8 for different compositions. The hydrodynamic radius of a polymer in solution in general depends on the polymer molecular weight $R_h \sim MW^{\nu}$ where ν is the Flory interaction parameter.[46] Polymer compositions P($C_5EG_6$) and P($C_8EG_{13}$) are close to theta-solvent conditions with $\nu \approx 0.5$ and P($C_4EG_4$) shows a good solvent behavior with $\nu \approx 0.6$ leading to more expanded coils. P($C_{10}EG_{22}$) with $\nu \approx 0.4$ seems to be partially collapsed like in a bad solvent.

Another intriguing observation we can see in Figure 8 is the clear change of the hydrodynamic size with the composition. The hydrodynamic radius increases with increasing the unit sizes for the compositions P($C_4EG_4$), P($C_5EG_6$) and P($C_8EG_{13}$). This might be related to an increased hydrophilic/hydrophobic unit ratio and, consequently, a more "PEG-like" behavior. The P($C_{10}EG_{22}$) polymer declines to smaller sizes than the trend suggests. This is a first indication of the hydrocarbon units interaction which leads to the formation of loops (see Figure 13) with a smaller hydrodynamic radius as discussed in the explanations related to Figure 10.

In order to examine the change of ν on approaching the CPT, we studied the dependence of the solvent quality on temperature. In particular we analyzed the temperature dependence of ν for the P($C_8EG_{13}$) (see Figure 8 insert). The maximum temperature is determined by the CPT of the largest molecular weight polymer so most of the polymers were well below the CPT. We found that there is no significant change in *ν*, respectively in the solvent quality, in the measured temperature range.

To examine the molecular structure of the polymers and the temperature behavior in more detail we performed SANS measurements with an extended Q-range for polymers P($C_8EG_{13}$) and P($C_4EG_4$) at several temperatures. Figure 9 shows SANS data for two molecular weights of P($C_8EG_{13}$) from well below to well above the CPT. At low temperatures the scattering pattern indicates a single chain behavior well described by a Debye-like function at lower Q. The aggregation, as indicated by an increase of intensity at low Q, starts slightly below the measured CPT, (CPT = 41°C for 21 kg/mol, CPT = 60°C for 4.7 kg/mol). Extracting the radius of gyration $R_g$ (see Figure 9B, inset) of the single chain component we observe first a slight drop in $R_g$ at the CPT, which is followed by a significant drop above the measured CPT. This indicates the expected collapse of the single chain structure.

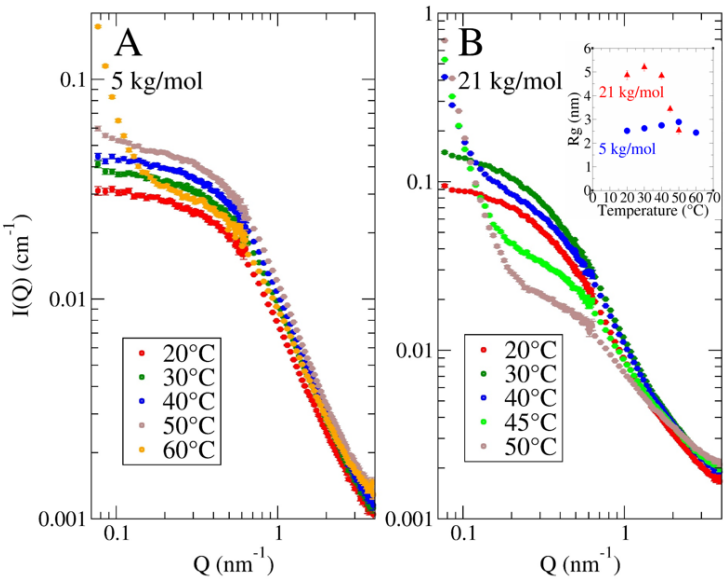


*Figure 9. SANS data for the AAPs at different temperatures for a concentration of 10mg/mL in $D_2O$. A: $P(C_8EG_{13})5k$; B: $P(C_8EG_{13})21k$. The insert shows the temperature dependence of $R_g$ for both AAPs. The values are obtained from fits with the wormlike-chain model which is described in the SI. The fits are shown in Figure S5.*

Taking a closer look at the high Q behavior in a Kratky plot $I(Q)Q^2$ vs. Q demonstrates a quite complex structure on length scales of unit sizes that deviates from simple polymer behavior as presented in Figure 10. The scattering pattern clearly deviates from a simple Gaussian polymer behavior. For a Gaussian polymer in a Kratky representation a constant value for $I(Q)Q^2$ is expected, which reflects a power law $\sim Q^{-2}$ for intermediate Q-values. Instead, we observe a remarkable structural peak around 1 nm$^{-1}$ followed by a plateau-like behavior at intermediate Q in some cases and finally a linear increase at high Q. As presented in Figure 10A for low MWs of $P(C_4EG_4)$ and $P(C_8EG_{13})$ we observe a continuous smooth increase to high Q, while for larger MW a plateau is observed. For the longest $P(C_4EG_4)$ chains with MW of 33 kg/mol an additional peak is visible.

The broken lines show a fit with a wormlike chain model.[47] The wormlike chain model considers a persistence length that describes the local stiffness of the chain. This leads to the linear increase at high Q which is independent of MW. The resulting persistence lengths for the lowest MW are in the range of 0.7 – 1 nm which is slightly larger than the value of 0.6 nm found for PEG. However, we cannot completely exclude that there is no influence of the loops which can affect the fit results. Figure 10B shows the temperature series from Figure 9A with the corresponding fits to the wormlike chain model. For lower temperatures we observe excellent agreement with the data, while for T=50°C a plateau comparable to high MW seems to evolve. The plateau value decreases for 60°C indicating an increase of the segment length[48] above the transition temperature. For 50°C and 60°C the high Q slope is stronger increasing compared to low temperatures. Figure 10C shows a temperatures series for $P(C_8EG_{13})$ MW of 21k with a pronounced plateau. With increasing temperature the plateau is first rising with a clear peak, decreases above 30°C and vanishes on a lower level above 45˚C. While increasing intensity indicates reduced segment length, vice versa, the peak with the following plateau is characteristic for loops or branched structures.[48] We fitted correspondingly the most

pronounced structure at T=30°C with a polymer ring model[49] including polydispersity as a proof of concept for the loops to describe the peak and the following plateau. From the fit an $R_g$ value of 3.9 nm was calculated and a polydispersity of 0.6 nm. Polymer models that include the loops and the wormlike chain behavior at higher Q are not available. We conclude that the plateau and corresponding peaks as a deviation from the wormlike chain model is due to loop formation of the polymer chain with itself due to attractive interaction between hydrophobic units (Figure 13). The loop formation depends on the attraction strength between the hydrophobic units but also on the ability of the polymer to bend. As the effect seems to be smaller for low MW we conclude that these chains are too short to form loops at least at lower temperatures. It should be mentioned that the high Q increase in a Kratky plot expected for polymer models with excluded volume (including polymer ring models) alone cannot explain the observed linear increase. Nevertheless excluded volume effects might partially contribute.

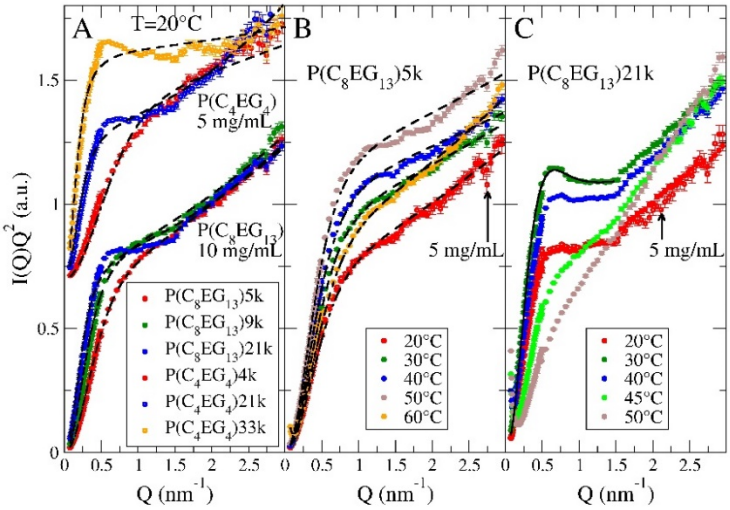


*Figure 10 Kratky plots of the SANS data in $D_2O$ at a concentration of 10 mg/mL and 5 mg/mL as indicated. A: Different molecular weights for the polymers $P(C_4EG_4)$ and $P(C_8EG_{13})$ at 20˚C; B: $P(C_8EG_{13})$5k at indicated temperatures.; C: $P(C_8EG_{13})$21k at indicated temperatures. Solid lines represent fits with a polymer ring model. Broken lines represent in all plots fit results from a wormlike chain model.*

With increasing the hydrophobic unit length a strong extension of the PEG units is required to make the polymers fully water-soluble (see Figure 4 and SI, Table S7). Even the polymers having very hydrophobic $C_{14}$ or $C_{20}$ units can be solubilized in combination with large enough PEG units as single chains. For example, the $P(C_{14}EG_{47})$ and $P(C_{20}EG_{240})$ are not fully soluble in water at room temperature whereas the $P(C_{14}EG_{103})$ and $P(C_{20}EG_{1000})$ solubilize completely.

## Micellar structures

When we gradually decrease the EG length while still keeping the polymers water-soluble, the polymers tend to form more compact structures which depend both on the hydrophobic unit length and the hydrophilic/hydrophobic unit length ratio. Figure 11 represents the SAXS results for polymers with $C_{14}$ and $C_{20}$ hydrophobic units. $P(C_{14}EG_{103})$48k represents an example

of a water-soluble polymer which shows the behavior of worm-like chains (see Figure 11). Decreasing the hydrophilic unit by about half leads to the polymer P($C_{14}EG_{47}$). Here only the fraction with the MW=16 kg/mol is fully water soluble. This polymer shows more compact structures characterized by the intensity drop at high Q which is more pronounced above 0.8 $nm^{-1}$ in the Kratky plot. In the intermediate Q-range the scattering curve indicates less compact structures compared to the spheres. Although the Gunier region is not reached for this sample, the overall structure size is larger than the size corresponding to the minimas at the Kratky plot. Therefore, we assume the formation of small mostly hydrophobic regions connected to each other by PEG units and forming as a whole a partially collapsed polymer chain (see Figure 13). Increasing the hydrophobic length to $C_{20}$ leads to the polymer P($C_{20}EG_{47}$). As all the P($C_{20}EG_{47}$) polymers are not fully water-soluble, the soluble part of the polymer P($C_{20}EG_{47}$)32k was taken for the measurement. The molecular weight of this polymer is 16 kg/mol and the concentration is 6 mg/mL. For this polymer the scattering pattern is more distinct than for the P($C_{14}EG_{47}$) polymers and can be well described by a micellar core-shell structure with an inhomogeneous core (see SI). Fitting with this model (black line) gives the core size of 3.7 nm and a diffuse shell with low contrast of about 5 nm thickness. In order to describe the scattering intensity at high Q, inhomogeneities must be included in the core. A core having the size of 3.7 nm cannot be built exclusively from the hydrophobic units only. We assume that it consists of the hydrophobic units, which form high contrast inhomogeneities and are embedded in a PEG-rich, low contrast matrix. We assume that the shell consists of a few PEG chains which are either loops or chain ends. However, an estimation of the shell density is difficult due to a low contrast of PEG to water for SAXS. As the radius of gyration of a respective 16 kg/mol PEG in water is about 6 nm,[50] we expect no more than a few polymer chains per micelle. A schematic view of the described micelle is presented in Figure 13. The soluble fractions of the polymers P($C_{20}EG_{103}$) and P($C_{20}EG_{240}$) also show the formation of micellar structures, similar to P($C_{20}EG_{47}$). A more precise model for the core is given later in the part about polymer gels.

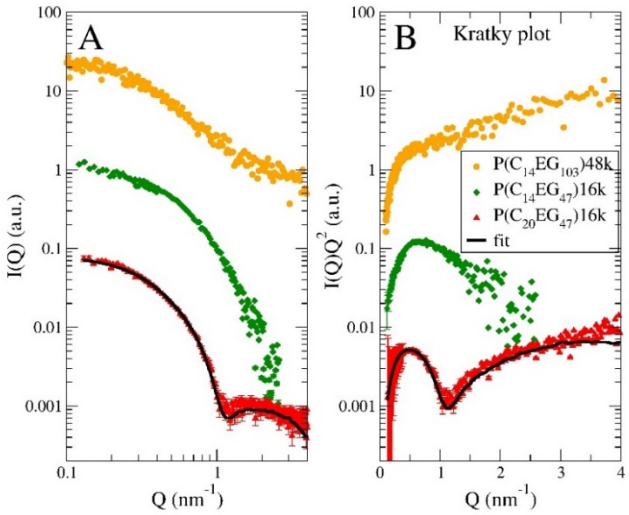


*Figure 11. A: SAXS curves for the polymers with long hydrophilic and hydrophobic units. The polymers were measured in water at concentration of 10 mg/mL for P($C_{14}EG_{103}$) and P($C_{14}EG_{47}$), and 6 mg/mL for P($C_{20}EG_{47}$). The intensity is scaled for convenience. The black lines show the fits with the core-shell model containing inhomogeneous cores. B: the same data are shown in a Kratky representation.*

## Gels

We studied the gel samples of various polymer concentrations and compositions by SAXS. Figure 12 compares the experimental SAXS results for the polymers P($C_{20}EG_{47}$), P($C_{20}EG_{103}$) and P($C_{20}EG_{240}$). The scattering results can be described on the basis of inhomogeneous core-shell particles as in the cases of micellar solutions. The resulting form factor *F*(Q) was combined with the Percus-Yevick structure factor *S(Q)* which describes the particle arrangement in a fluid order leading to structure factor peaks. For the P($C_{20}EG_{47}$)113k polymers a size polydispersity of the cores had to be included to describe the scattering pattern. For the other polymers the shape anisotropy had to be included in order to suppress the higher order structure factor peaks. The increase at low Q can be described by domain scattering, which was added as a low-Q power law *G(Q)* (see SI for details). The final scattering function was calculated as

$$I(Q) = S(Q)F(Q) + G(Q) \quad (2)$$

In the dry state the polymers are organized in a lamellar structure which is formed by the crystalline PEG and the hydrocarbon layers in between (see Figure S6). However, already at a water content of 50 wt% the core-shell structures evolve and can be fitted by the model described above (see Figure 12 A1 and A2). The two peaks of the experimental data correspond to the first structure factor peaks. At this concentration the distance between the cores is almost equal to the core size, so the structure factor has a very small value at low Q. The first order peak position is very similar to the position of the form-factor minima at about 1 $nm^{-1}$, which give very high and distinct peaks of $S(Q)F(Q)$. The second order peak indicates a more ordered structure and therefore is not satisfactorily described by the Percus-Yevick structure factor. Figure 12 A3 shows the 50 wt% gels varying the PEG length. The peak positions shift to lower Q with increasing PEG length due to a larger distance between the cores. Taking into account the same polymer concentration and the same intensity drop at the left side of the peaks we can conclude that the distance between the cores changes mainly due to the increased size of the cores. We explain the decrease of the scattering intensity with increasing PEG length by the reduced hydrocarbon unit fraction in the polymer chains and, consequently, the lower contrast of the cores. Figure 12 B1 and B2 show the gel model for the fully swollen P($C_{20}EG_{47}$)113k polymer at a concentration of 15 wt%. Although the scattering pattern looks different compared to the 50 wt% sample, it can be described with the same model. At higher swelling the volume fraction of the cores decreases which leads to a higher value of the S(Q) at low Q and the peaks shift to lower Q compared to the F(Q) minima. This results in a first order S(Q) peak overlapping with the F(Q) shoulder and a well pronounced second order S(Q) peak. Figure 12 B3 shows again the polymers having different PEG lengths at a concentration of 15 wt%. The first order peak again shifts to lower Q as expected, and the second order peak vanishes for the polymers with longer PEG units. Figure 12 C1 and C2 show the gel model for the polymer P($C_{20}EG_{103}$)161k at maximum swelling which corresponds to a polymer concentration of 8 wt%. The second order S(Q) peak also disappears. Increased shape anisotropy of the cores with increasing the PEG unit length leads to a suppression of all higher order peaks of the S(Q).[51] Figure 12 C3 shows the changes for increasing PEG length. The first order peak shows a shift and becomes less pronounced which is expected for low core volume

fractions at high swelling. We notice that both, the core size and the structural arrangement of the cores are independent of the polymer MW. This is reasonable because in a macroscopic gel the polymer extension is larger than the core-core distance allowing the polymer chain to interconnect cores.

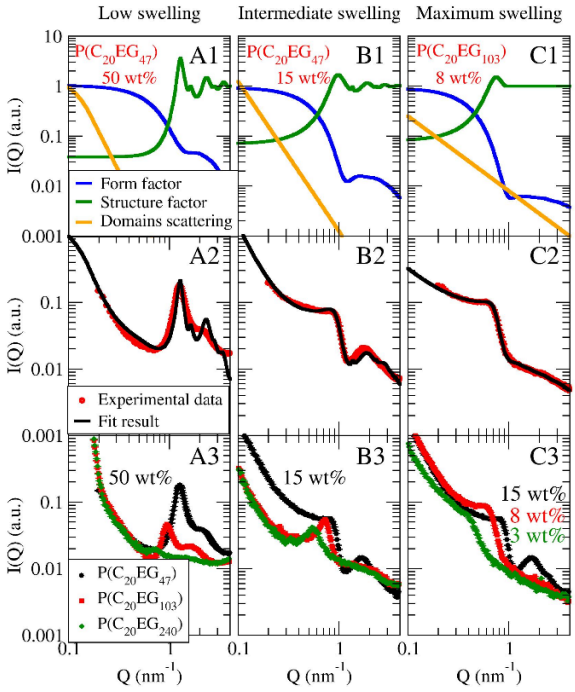


*Figure 12. SAXS curves and gel models for three different polymer concentrations and compositions. A1, A2: model for the polymer P($C_{20}EG_{47}$)113k of the concentration 50 wt%. A3: Comparison of the SAXS curves for the polymers with different EG lengths at 50 wt% concentration. B1, B2: model for the polymer P($C_{20}EG_{47}$)113k at 15 wt% concentration. B3: Comparison of the SAXS curves for the polymers with different EG lengths at 15 wt% concentration. C1, C2: model for the polymer P($C_{20}EG_{103}$)161k at 8 wt% concentration. C3: Comparison of the SAXS curves for the polymers with different EG lengths at 8 wt% concentration (maximum swelling).*

In order to estimate the water content and the number of hydrophobic/hydrophilic repeat units inside a core we chose a model for the fully swollen P($C_{20}EG_{47}$)113k gel (Figure 12 B1 and B2). The form factor gives a core radius of 3.3 nm and a core volume fraction of 35%. Taking into account the polymer concentration of 15% at the maximum swelling degree we find that the concentration of the polymer in the core is 43%. This allows us to estimate the number of hydrophobic/hydrophilic units per core. Considering the volume of such a unit of 3.3 $nm^3$, we calculated 19.6 hydrophobic/hydrophilic units per core. For the polymer P($C_{20}EG_{47}$)113k which makes the strongest gel, this value corresponds to 0.41 polymer chains. Therefore, the cores must be strongly interconnected by the polymer chains, which explains the high mechanical stability we observe for these gels (see Figure S4).

## 4. Discussion of the structural properties

Exceeding a certain threshold for the EG unit length, the AAPs solubilize as free chains with a slightly larger persistence length than that for PEG.[52] Intrachain loop formation is observed for these polymers (see Figure 13). We suppose that the ability of AAPs to form at least

metastable loops is attributed to attractive interactions between the hydrophobic units. As AAPs may form inner loops between any of the hydrophobic units of a chain, the probability for loop formation increases with increasing polymer molecular weight. The opposite effect of the molecular weight was found for telechelic polymers,[53] where micellar loop formation is related to end-end loops which is less probable for longer chains. Due to loop formation, the AAPs form less extended coils than expected for a Gaussian chain. An increased loop formation with increasing temperature close to the transition point shows that the phase transition of the AAPs is a continuous process which starts before the chain collapse happens. Increasing the length of the hydrophobic unit leads to stronger hydrophobic interactions and requires a dramatic increase of the EG unit to keep the polymers water-soluble. When the EG length is not long enough, the hydrophobic interactions provoke the formation of micelles containing multiple hydrophobic contacts. As a result, the micellar core consists of several small hydrophobic regions incorporated in a PEG-rich matrix, containing only a small amount of water (Figure 13). In order to understand such behavior, we compare our micelles with telechelic polymers studies by Alami et. al.[53] In this work PEGs were used which contain hydrocarbon units at the chain ends. The ability to form loops, which leads to the formation of micelles, is related to the change in free energy which can be estimated[53] as

$$\Delta G \approx 1.5RTln(n) - 0.4RTm \qquad (3)$$

where n is the number of EG monomers in the hydrophilic unit and m is the number of $CH_2$ groups at a chain end. The first term is attributed to the entropy loss of the PEG chains due to the loop formation, and the second term describes the gain in free energy when the hydrophobic tails associate. This implies that at short alkyl chains and long enough PEG the entropy term dominates which leads to free polymer chains. At longer alkyl chains and/or shorter PEG, when the second term dominates, strong hydrophobic interactions lead to the formation of stable flower-like micelles. It was reported[54] that in the intermediate state, when the entropy term dominates but the formation of loops still has a reasonable probability, the micelle formation takes place but not all of the hydrophobic chain ends are located in the micellar core.

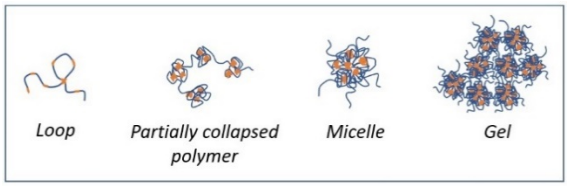


*Figure 13. Structures of AAPs in water*

The AAP P($C_{20}EG_{47}$) forming the most defined micelles can be described in a simple picture as a sequence of telechelic $C_{10}EG_{47}C_{10}$ units. $\Delta G$ for this polymer has a positive value, which explains why the AAP micelles have no single hydrophobic core. Furthermore, water molecules are highly polar. Their dipole moment is 1.84 debye, compared to a value of 1.04 debye for a monomer unit in PEG.[55] This makes the observed PEG-rich core structure of the AAP micelles more favorable compared to the structure where the hydrophobic regions are embedded in a water-rich environment.

Similar structures were found in simulation studies. Depending on the segment lengths, their ratio, the solvent quality as well as other criteria a large variety of micellar structures were found,[17,18,20] among them multi-core micelles, where the cores are surrounded by a rather dense shell of the hydrophilic polymer. In experimental studies to our knowledge, such structures have not been reported so far. This also applies to AAPs having polymeric hydrophobic and hydrophilic units. In a study where alternating amphiphilic PEO/PPO multiblock copolymers were used, which contain polymeric hydrophobic PPO blocks,[14] the multiblock copolymers form flower-like structures under loop formation of the PEO blocks. This is understandable as the hydrophobic interactions are stronger and the spacial restrictions for loop formation are smaller than in the case of low MW hydrophobic units. It is interesting to observe that the gels formed by the AAPs with long hydrophobic and hydrophilic units have the same structural features as in the micelles (Figure 13). Moreover, these structures are independent of the polymer molecular weight. Our calculations show that there are about 20 hydrophobic/hydrophilic repeat units per one core. Especially for the polymers having a large number of hydrophobic/hydrophilic repeat units, one chain is located in more than one micellar core, increasing the number of crosslinks. The crosslinks between the cores are much stronger than for the telechelic polymers where only the chain ends must be pulled out of the core. This leads to a much higher mechanical stability and elasticity of the AAP gels compared to the gels made by telechelic polymers. The details are given in the SI. The gels always coexist with the micelles or free polymers of smaller molecular weight. In the case of free micelles the number of polymer chains per core is about 2.5, which allows them to stay single. A qualitatively similar phase diagram for the AAPs was reported in the simulation work by Hugouvieux V. et al.[19]

## 5. Conclusions

The synthesis of polyesters from dicarboxylic acids and PEG monomers represents a simple procedure to gain access to AAP, making a broad range of hydrophilic and hydrophobic unit lengths and compositions accessible. The variation of the lengths of the hydrophilic and hydrophobic blocks allows tuning the LCST between 3 and 83°C. For large PEG-units the copolymers are soluble as single chains. For longer hydrophobic units, i.e. $C_{14}$ and $C_{20}$, micelle and gel formation is observed. The formation of a pure alkyl micellar core is hindered by the conformational restrictions resulting from the alternating arrangement of the hydrophilic and hydrophobic units. As a consequence, the micellar cores consist of several small hydrophobic regions embedded in a PEG-rich and water-poor matrix. The micellar cores represent the nodes of the network structure of the macroscopic gels. The strongly swollen gels show a high degree of mechanical stability (see Figure S4). We also found that the polymer forms lyotropic liquid crystals as demonstrated for P($C_{20}EG_{47}$)113k at 50 wt% concentration (Figure S7). We observe a highly ordered crystalline structure with peaks up to 4$^{th}$ order (bcc or simple cubic) which melts at higher temperatures). This makes the material interesting for rheological experiments as this allows quenching of e.g. shear oriented structures. The study demonstrates how the structure of alternating amphiphilic copolymers can be systematically varied to adjust the hydrophilic/hydrophobic balance and thus the solution and self-assembly properties. Copolymers with a larger hydrophobic fraction are expected to be compatible with

hydrophobic environments such as lipid membranes, which can be utilized in biological applications.[56]

## 6. Acknowledgments

The authors thank Ann Gogolashvili and Veronika Khodyreva for performing some of the presented DLS measurements in the frame of summer program of International Helmholtz Research School (IHRS) of Biophysics and Soft Matter. The authors thank IHRS for Biophysics and Soft Matter for organizing the mentioned above summer program.

## References

(1) Holder, S. J.; Sommerdijk, N. A. J. M. New Micellar Morphologies from Amphiphilic Block Copolymers: Disks, Toroids and Bicontinuous Micelles. *Polymer Chemistry*. Royal Society of Chemistry April 12, 2011, pp 1018–1028. https://doi.org/10.1039/c0py00379d.

(2) Lund, R.; Willner, L.; Monkenbusch, M.; Panine, P.; Narayanan, T.; Colmenero, J.; Richter, D. Structural Observation and Kinetic Pathway in the Formation of Polymeric Micelles. *Phys. Rev. Lett.* **2009**, *102* (18), 188301. https://doi.org/10.1103/PhysRevLett.102.188301.

(3) Uramoto, K.; Takahashi, R.; Terao, K.; Sato, T. Local and Global Conformations of Flower Micelles and Flower Necklaces Formed by an Amphiphilic Alternating Copolymer in Aqueous Solution. *Polym. J.* **2016**, *48* (8), 863–867. https://doi.org/10.1038/pj.2016.49.

(4) Ueda, M.; Hashidzume, A.; Sato, T. Unicore-Multicore Transition of the Micelle Formed by an Amphiphilic Alternating Copolymer in Aqueous Media by Changing Molecular Weight. *Macromolecules* **2011**, *44* (8), 2970–2977. https://doi.org/10.1021/ma102635y.

(5) Di Cola, E.; Plucktaveesak, N.; Waigh, T. A.; Colby, R. H.; Tan, J. S.; Pyckhout-Hintzen, W.; Heenan, R. K. Structure and Dynamics in Aqueous Solutions of Amphiphilic Sodium Maleate-Containing Alternating Copolymers. *Macromolecules* **2004**, *37* (22), 8457–8465. https://doi.org/10.1021/ma049260h.

(6) Rackaitis, M.; Strawhecker, K.; Manias, E. RAPID COMMUNICATION Water-Soluble Polymers with Tunable Temperature Sensitivity: Solution Behavior*. **2002**. https://doi.org/10.1002/polb.10284.

(7) Goswami, K. G.; Mete, S.; Chaudhury, S. S.; Sar, P.; Ksendzov, E.; Mukhopadhyay, C. Das; Kostjuk, S. V.; De, P. Self-Assembly of Amphiphilic Copolymers with Sequence-Controlled Alternating Hydrophilic–Hydrophobic Pendant Side Chains. *ACS Appl. Polym. Mater.* **2020**, *2* (5), 2035–2045. https://doi.org/10.1021/acsapm.0c00204.

(8) Tomalino, L. M.; Voronov, A.; Kohut, A.; Peukert, W. Study of Amphiphilic Polyester Micelles by Hyper-Rayleigh Scattering: Invertibility and Phase Transfer. *J. Phys. Chem. B* **2008**, *112* (20), 6338–6343. https://doi.org/10.1021/jp710499z.

(9) Heitz, C.; Pendharkar, S.; Prud'Homme, R. K.; Kohn, J. A New Strictly Alternating Comblike Amphiphilic Polymer Based on PEG. 1. Synthesis and Associative Behavior of a Low Molecular Weight Sample. *Macromolecules* **1999**, *32* (20), 6652–6657. https://doi.org/10.1021/ma991158a.

(10) Heitz, C.; Prud'Homme, R. K.; Kohn, J. A New Strictly Alternating Comblike Amphiphilic Polymer Based on PEG. 2. Associative Behavior of a High Molecular Weight Sample and Interaction with SDS. *Macromolecules* **1999**, *32* (20), 6658–6667. https://doi.org/10.1021/ma9911593.

(11) Xu, Q.; Li, S.; Yu, C.; Zhou, Y. Self-Assembly of Amphiphilic Alternating Copolymers. *Chem. - A Eur. J.* **2019**, *25* (17), 4255–4264. https://doi.org/10.1002/chem.201804067.

(12) Horiuchi, T.; Rikiyama, K.; Sakanaya, K.; Sanada, Y.; Watanabe, K.; Aida, M.; Katsumoto, Y. Effect of Molecular Weight on Cloud Point of Aqueous Solution of Poly (Ethylene Oxide)– Poly (Propylene Oxide) Alternating Multiblock Copolymer. *J. Oleo Sci.* **2020**, *69* (5), 449–453. https://doi.org/10.5650/jos.ess20026.

(13) Horiuchi, T.; Sakai, T.; Sanada, Y.; Watanabe, K.; Aida, M.; Katsumoto, Y. Association Behavior of Poly(Ethylene Oxide)-Poly(Propylene Oxide) Alternating Multiblock Copolymers in Water toward Thermally Induced Phase Separation. *Langmuir* **2017**, *33* (51), 14649–14656. https://doi.org/10.1021/acs.langmuir.7b02810.

(14) Rikiyama, K.; Horiuchi, T.; Koga, N.; Sanada, Y.; Watanabe, K.; Aida, M.; Katsumoto, Y. Micellization of Poly(Ethylene Oxide)-Poly(Propylene Oxide) Alternating Multiblock Copolymers in Water. *Polymer (Guildf).* **2018**, *156*, 102–110. https://doi.org/10.1016/j.polymer.2018.09.047.

(15) Hadjiantoniou, N. A.; Triftaridou, A. I.; Kafouris, D.; Gradzielski, M.; Patrickios, C. S. Synthesis and Characterization of Amphiphilic Multiblock Copolymers: Effect of the Number of Blocks on Micellization. *Macromolecules* **2009**, *42* (15), 5492–5498. https://doi.org/10.1021/ma900554k.

(16) Hadjiantoniou, N. A.; Krasia-Christoforou, T.; Loizou, E.; Porcar, L.; Patrickios, C. S. Alternating Amphiphilic Multiblock Copolymers: Controlled Synthesis via RAFT Polymerization and Aqueous Solution Characterization. *Macromolecules* **2010**, *43* (6), 2713–2720. https://doi.org/10.1021/ma902709p.

(17) De Silva, C. C.; Leophairatana, P.; Ohkuma, T.; Koberstein, J. T.; Kremer, K.; Mukherji, D. Sequence Transferable Coarse-Grained Model of Amphiphilic Copolymers. *J. Chem. Phys.* **2017**, *147* (6), 64904. https://doi.org/10.1063/1.4997638.

(18) Hogouvieux, V.; Axelos, M. A. V.; Kolb, M. Amphiphilic Multiblock Copolymers: From Intramolecular Pearl Necklace to Layered Structures. *Macromolecules* **2009**, *42* (1), 392–400. https://doi.org/10.1021/ma801337a.

(19) Hugouvieux, V.; Axelos, M. A. V.; Kolb, M. Micelle Formation, Gelation and Phase Separation of Amphiphilic Multiblock Copolymers†. *Soft Matter* **2011**, *7* (6), 2580–2591. https://doi.org/10.1039/c0sm01018a.

(20) Cooke, I. R.; Williams, D. R. M. Collapse Dynamics of Block Copolymers in Selective Solvents: Micelle Formation and the Effect of Chain Sequence. *Macromolecules* **2003**, *36* (6), 2149–2157. https://doi.org/10.1021/ma020741f.

(21) Li, S.; Yu, C.; Zhou, Y. Phase Diagrams, Mechanisms and Unique Characteristics of Alternating-Structured Polymer Self-Assembly via Simulations. *Sci. China Chem.* **2019**, *62* (2), 226–237. https://doi.org/10.1007/s11426-018-9360-3.

(22) Sung, Y. K.; Kim, S. W. Recent Advances in Polymeric Drug Delivery Systems. *Biomaterials Research*. BioMed Central Ltd June 6, 2020, pp 1–12. https://doi.org/10.1186/s40824-020-00190-7.

(23) Chatterjee, S.; Hui, P. C. L.; Kan, C. wai. Thermoresponsive Hydrogels and Their Biomedical Applications: Special Insight into Their Applications in Textile Based Transdermal Therapy. *Polymers*. MDPI AG April 27, 2018, p 480. https://doi.org/10.3390/polym10050480.

(24) Sponchioni, M.; Capasso Palmiero, U.; Moscatelli, D. Thermo-Responsive Polymers: Applications of Smart Materials in Drug Delivery and Tissue Engineering. *Materials Science and Engineering C*. Elsevier Ltd September 1, 2019, pp 589–605. https://doi.org/10.1016/j.msec.2019.04.069.

(25) Vanparijs, N.; Nuhn, L.; De Geest, B. G. Transiently Thermoresponsive Polymers and Their Applications in Biomedicine. *Chemical Society Reviews*. Royal Society of Chemistry February 21, 2017, pp 1193–1239. https://doi.org/10.1039/c6cs00748a.

(26) Frazar, E. M.; Shah, R. A.; Dziubla, T. D.; Hilt, J. Z. Multifunctional Temperature-Responsive Polymers as Advanced Biomaterials and Beyond. *Journal of Applied Polymer Science*. John Wiley and Sons Inc. July 5, 2020, p 48770. https://doi.org/10.1002/app.48770.

(27) Halperin, A.; Kröger, M.; Winnik, F. M. Poly(N-Isopropylacrylamide) Phase Diagrams: Fifty Years of Research. *Angew. Chemie - Int. Ed.* **2015**, *54* (51), 15342–15367. https://doi.org/10.1002/anie.201506663.

(28) Plamper, F. A.; Richtering, W. Functional Microgels and Microgel Systems. *Acc. Chem. Res.* **2017**, *50* (2), 131–140. https://doi.org/10.1021/acs.accounts.6b00544.

(29) Roy, D.; Brooks, W. L. A.; Sumerlin, B. S. New Directions in Thermoresponsive Polymers. *Chem. Soc. Rev.* **2013**, *42* (17), 7214–7243. https://doi.org/10.1039/c3cs35499g.

(30) Weber, C.; Hoogenboom, R.; Schubert, U. S. Temperature Responsive Bio-Compatible Polymers Based on Poly(Ethylene Oxide) and Poly(2-Oxazoline)S. *Prog. Polym. Sci.* **2012**, *37* (5), 686–714. https://doi.org/10.1016/J.PROGPOLYMSCI.2011.10.002.

(31) Louai, A.; Sarazin, D.; Pollet, G.; François, J.; Moreaux, F. Properties of Ethylene Oxide-Propylene Oxide Statistical Copolymers in Aqueous Solution. *Polymer (Guildf).* **1991**, *32* (4), 703–712. https://doi.org/10.1016/0032-3861(91)90484-Z.

(32) Mangold, C.; Obermeier, B.; Wurm, F.; Frey, H. From an Epoxide Monomer Toolkit to Functional PEG Copolymers with Adjustable LCST Behavior. *Macromol. Rapid Commun.* **2011**, *32* (23), 1930–1934. https://doi.org/10.1002/marc.201100489.

(33) Samanta, S.; Bogdanowicz, D. R.; Lu, H. H.; Koberstein, J. T. Polyacetals: Water-Soluble, PH-Degradable Polymers with Extraordinary Temperature Response. *Macromolecules* **2016**, *49* (5), 1858–1864. https://doi.org/10.1021/acs.macromol.5b02304.

(34) Hövelmann, C. H.; Gooßen, S.; Allgaier, J. Scale-Up Procedure for the Efficient Synthesis of Highly Pure Cyclic Poly(Ethylene Glycol). *Macromolecules* **2017**, *50* (11), 4169–4179. https://doi.org/10.1021/acs.macromol.7b00361.

(35) Maier-Leibnitz Zentrum Forschungszentrum Jülich, H.; Maier-Leibnitz Zentrum, H. KWS-1: Small-Angle Scattering Diiractometer. *J. large-scale Res. Facil.* **2015**, *1* (0), 28. https://doi.org/10.17815/jlsrf-1-26.

(36) Feoktystov, A. V.; Frielinghaus, H.; Di, Z.; Jaksch, S.; Pipich, V.; Appavou, M. S.; Babcock, E.; Hanslik, R.; Engels, R.; Kemmerling, G.; Kleines, H.; Ioffe, A.; Richter, D.; Brückel, T. KWS-1 High-Resolution Small-Angle Neutron Scattering Instrument at JCNS: Current State. *J. Appl. Crystallogr.* **2015**, *48* (1), 61–70. https://doi.org/10.1107/S1600576714025977.

(37) V. Pipich. QtiKWS http://www.qtisas.com/qtikws (accessed Jun 18, 2021).

(38) Biehl, R. Jscatter, a Program for Evaluation and Analysis of Experimental Data. *PLoS One* **2019**, *14* (6). https://doi.org/10.1371/journal.pone.0218789.

(39) Kentzinger, E.; Krutyeva, M.; Rücker, U. GALAXI: Gallium Anode Low-Angle x-Ray Instrument. *J. large-scale Res. Facil. JLSRF* **2016**, *2* (0), 61. https://doi.org/10.17815/jlsrf-2-109.

(40) Armstrong, A.; Li, W. N,N ′-Carbonyldiimidazole . In *Encyclopedia of Reagents for Organic Synthesis*; John Wiley & Sons, Ltd, 2007. https://doi.org/10.1002/9780470842898.rc024.pub2.

(41) Dunn, P. J.; Hoffmann, W.; Kang, Y.; Mitchell, J. C.; Snowden, M. J. A Comparison of Catalysts to Promote Imidazolide Couplings Including the Identification of 2-Hydroxy-5-Nitropyridine as a New, Safe, and Effective Catalyst. *Org. Process Res. Dev.* **2005**, *9* (6), 956–961. https://doi.org/10.1021/op0580062.

(42) Peng, Z.; Wong, J. W.; Hansen, E. C.; Puchlopek-Dermenci, A. L. A.; Clarke, H. J. Development of a Concise, Asymmetric Synthesis of a Smoothened Receptor (Smo) Inhibitor: Enzymatic Transamination of a 4-Piperidinone with Dynamic Kinetic Resolution. *Org. Lett.* **2014**, *16* (3), 860–863. https://doi.org/10.1021/ol403630g.

(43) Saeki, S.; Kuwahara, N.; Nakata, M.; Kaneko, M. Upper and Lower Critical Solution Temperatures in Poly (Ethylene Glycol) Solutions. *Polymer (Guildf).* **1976**, *17* (8), 685–689. https://doi.org/10.1016/0032-3861(76)90208-1.

(44) Tompa, H. Phase Relationships in Polymer Solutions. *Trans. Faraday Soc.* **1949**, *45* (0), 1142–1152. https://doi.org/10.1039/TF9494501142.

(45) Hammouda, B.; Ho, D. L.; Kline, S. Insight into Clustering in Poly(Ethylene Oxide) Solutions. *Macromolecules* **2004**, *37* (18), 6932–6937. https://doi.org/10.1021/ma049623d.

(46) Doi, M.; Edwards, S. F. *The Theory of Polymer Dynamics*; Birman, J., Edwards, S. F., LLewellyn Smith, C. H., Rees, M., Eds.; Oxford University Press, USA: Oxford, 1988. https://doi.org/10.1016/S1359-0286(96)80106-9.

(47) Kholodenko, A. L. Analytical Calculation of the Scattering Function for Polymers of Arbitrary Flexibility Using the Dirac Propagator. *Macromolecules* **1993**, *26* (16), 4179–

4183. https://doi.org/10.1021/ma00068a017.

(48) Benoît, H.; Joanny, J. F.; Hadziioannou, G.; Hammouda, B. Scattering by Linear, Branched, and Copolymer Chain Molecules for Large Scattering Vectors. *Macromolecules* **1993**, *26* (21), 5790–5795. https://doi.org/10.1021/ma00073a037.

(49) Hammouda, B. Form Factors for Branched Polymers with Excluded Volume. *J. Res. Natl. Inst. Stand. Technol.* **2016**, *121*, 139–164. https://doi.org/10.6028/jres.121.006.

(50) Kawaguchi, S.; Imai, G.; Suzuki, J.; Miyahara, A.; Kitano, T.; Ito, K. Aqueous Solution Properties of Oligo- and Poly(Ethylene Oxide) by Static Light Scattering and Intrinsic Viscosity. *Polymer (Guildf).* **1997**, *38* (12), 2885–2891. https://doi.org/10.1016/S0032-3861(96)00859-2.

(51) Kotlarchyk, M.; Chen, S.-H. Analysis of Small Angle Neutron Scattering Spectra from Polydisperse Interacting Colloids. *J. Chem. Phys.* **1983**, *79* (5), 2461. https://doi.org/10.1063/1.446055.

(52) Lee, H.; Venable, R. M.; MacKerell, A. D.; Pastor, R. W. Molecular Dynamics Studies of Polyethylene Oxide and Polyethylene Glycol: Hydrodynamic Radius and Shape Anisotropy. *Biophys. J.* **2008**, *95* (4), 1590–1599. https://doi.org/10.1529/biophysj.108.133025.

(53) Alami, E.; Almgren, M.; Brown, W.; François, J. Aggregation of Hydrophobically End-Capped Poly(Ethylene Oxide) in Aqueous Solutions. Fluorescence and Light-Scattering Studies. *Macromolecules* **1996**, *29* (6), 2229–2243. https://doi.org/10.1021/ma951174h.

(54) Zinn, T.; Willner, L.; Knudsen, K. D.; Lund, R. Self-Assembly of Mixtures of Telechelic and Monofunctional Amphiphilic Polymers in Water: From Clusters to Flowerlike Micelles. *Macromolecules* **2017**, *50* (18), 7321–7332. https://doi.org/10.1021/acs.macromol.7b01501.

(55) Yamaguchi, N.; Sato, M. Dipole Moment of Poly(Ethylene Oxide) in Solution and Its Dependence on Molecular Weight and Temperature. *Polym. J. 2009 418* **2009**, *41* (8), 588–594. https://doi.org/10.1295/polymj.pj2008232.

(56) Werner, M.; Sommer, J. U. Translocation and Induced Permeability of Random Amphiphilic Copolymers Interacting with Lipid Bilayer Membranes. *Biomacromolecules* **2015**, *16* (1), 125–135. https://doi.org/10.1021/bm501266x.